COLUMBIA UNIVERSITY
IN THE CITY OF NEW YORK
LAMONT-DOHERTY EARTH OBSERVATORY

November 3, 2008

To whom it may concern,

The following is a paper in the Proceedings of the [US] National Academy of Sciences. The methods described in this paper are proprietary. These methods are the property of Columbia University, with US patents pending. We will gladly share details of this method, and the ongoing modeling effort associated with it, in order to pursue the mutual benefit of testing this method. If the method is to be developed for commercial use, then separate arrangements must be made.

Sincerely,

Peter B. Kelemen
Arthur D. Storke Professor
Dept. of Earth & Environmental Sciences

peterk@ldeo.columbia.edu

In situ carbonation of peridotite for CO_2 storage

Peter B. Kelemen[1] and Jürg Matter

Lamont–Doherty Earth Observatory, Columbia University, Palisades, NY 10964

Edited by David Walker, Lamont–Doherty Earth Observatory of Columbia University, Palisades, NY, and approved September 22, 2008 (received for review June 17, 2008)

The rate of natural carbonation of tectonically exposed mantle peridotite during weathering and low-temperature alteration can be enhanced to develop a significant sink for atmospheric CO_2. Natural carbonation of peridotite in the Samail ophiolite, an uplifted slice of oceanic crust and upper mantle in the Sultanate of Oman, is surprisingly rapid. Carbonate veins in mantle peridotite in Oman have an average ^{14}C age of ≈26,000 years, and are not 30–95 million years old as previously believed. These data and reconnaissance mapping show that ≈10^4 to 10^5 tons per year of atmospheric CO_2 are converted to solid carbonate minerals via peridotite weathering in Oman. Peridotite carbonation can be accelerated via drilling, hydraulic fracture, input of purified CO_2 at elevated pressure, and, in particular, increased temperature at depth. After an initial heating step, CO_2 pumped at 25 or 30 °C can be heated by exothermic carbonation reactions that sustain high temperature and rapid reaction rates at depth with little expenditure of energy. In situ carbonation of peridotite could consume >1 billion tons of CO_2 per year in Oman alone, affording a low-cost, safe, and permanent method to capture and store atmospheric CO_2.

alteration and weathering | carbon capture | exothermic | carbon sequestration | mineral

Recognition that anthropogenic CO_2 input to the atmosphere has substantially increased atmospheric CO_2 concentration, and that increased CO_2 may drive rapid global warming, has focused attention on carbon capture and storage (1). One storage option is conversion of CO_2 gas to stable, solid carbonate minerals such as calcite ($CaCO_3$) and magnesite ($MgCO_3$) (2). Natural carbonation of peridotite by weathering and low-temperature alteration is common. Enhanced natural processes in situ may provide an important, hitherto neglected alternative to ex situ mineral carbonation "at the smokestack." In this article, we evaluate the rate of natural carbonation of mantle peridotite in the Samail ophiolite, Sultanate of Oman, and then show that under certain circumstances exothermic peridotite alteration (serpentinization, carbonation) can sustain high temperature and rapid reaction with carbonation up to 1 million times faster than natural rates, potentially consuming billions of tons of atmospheric CO_2 per year. In situ mineral carbonation for CO_2 storage should be evaluated as an alternative to ex situ methods, because it exploits the chemical potential energy inherent in tectonic exposure of mantle peridotite at the Earth's surface, does not require extensive transport and treatment of solid reactants, and requires less energy for maintaining optimal temperature and pressure.

Tectonically exposed peridotite from the Earth's upper mantle, and its hydrous alteration product serpentinite, have been considered promising reactants for conversion of atmospheric CO_2 to solid carbonate (3). However, engineered techniques for ex situ mineral carbonation have many challenges. Kinetics is slow unless olivine and serpentine reactants are ground to powder, heat-treated, and held at elevated pressure and temperature (4).* Pending further improvements, these approaches may be too expensive in financial terms and energy expenditures (5).

The potential for in situ mineral carbonation in peridotite is emphasized in the following simple calculation. There are ≈$2.9 \cdot 10^{15}$ kg of CO_2 in the atmosphere, up from a preindustrial value of perhaps $2.2 \cdot 10^{15}$ kg (6). In Oman, the Samail "ophiolite"—a thrust-bounded slice of oceanic crust and upper mantle—is >350 km long and ≈40 km wide, and it has an average thickness of ≈5 km (7). Of this volume ≈30% is mantle peridotite. Adding 1 wt% CO_2 to the peridotite would consume ¼ of all atmospheric CO_2, an amount approximately equivalent to the increase since the industrial revolution. Converting all Mg cations in the peridotite to carbonate would consume ≈$7 \cdot 10^{16}$ kg (77 trillion tons) of CO_2. Similarly large ophiolites are in Papua New Guinea (≈200 × 50 km in area), New Caledonia (≈150 × 40 km), and along the east coast of the Adriatic Sea (several ≈100 × 40 km massifs).

Mantle peridotite is ordinarily beneath the Earth's crust, >6 km below the seafloor and 40 km below the land surface. It is strongly out of equilibrium with air and water at the Earth's surface. Its exposure via large thrust faults along tectonic plate boundaries creates a reservoir of chemical potential energy. Fyfe (8) proposed that exothermic hydration (forming serpentine minerals) can heat peridotite. His idea has recently been invoked to explain the heat source for ≈90 °C fluids at the Lost City hydrothermal vent system near the Mid-Atlantic Ridge (9), and evaluated theoretically (10, 11). Below, we show that carbonation of peridotite generates more power than hydration because of larger enthalpy changes and faster reactions between 25 and 200 °C. Temperatures necessary for rapid reaction can be sustained via exothermic carbonation, instead of an external heat source.

Natural Peridotite Hydration and Carbonation

Mantle peridotite is composed largely of the minerals olivine [$(Mg,Fe)_2SiO_4$] and pyroxene [$(Ca,Mg,Fe)_2Si_2O_6$], which react with H_2O and CO_2 near the Earth's surface to form hydrous silicates (serpentine), Fe-oxides (magnetite), and carbonates (calcite, magnesite, and dolomite). Such reactions may generally be formulated as:

$$\underset{\text{Mg-olivine}}{2Mg_2SiO_4} + \underset{\text{Mg-pyroxene}}{Mg_2Si_2O_6} + 4H_2O = \underset{\text{serpentine}}{2Mg_3Si_2O_5(OH)_4} \quad [1]$$

$$\underset{\text{Mg-olivine}}{Mg_2SiO_4} + 2CO_2 = \underset{\text{magnesite}}{2MgCO_3} + \underset{\text{quartz}}{SiO_2} \quad [2a]$$

$$\underset{\text{Mg-olivine}}{Mg_2SiO_4} + \underset{\text{CaMg-pyroxene}}{CaMgSi_2O_6} + 2CO_2 + 2H_2O = \underset{\text{serpentine}}{Mg_3Si_2O_5(OH)_4} + \underset{\text{calcite}}{CaCO_3} + \underset{\text{magnesite}}{MgCO_3} \quad [2b]$$

Author contributions: P.B.K. and J.M. designed research, performed research, analyzed data, and wrote the paper.

Conflict of interest statement: P.B.K. and J.M. have a preliminary patent filing for the technique of heating peridotite to achieve self-sustaining, rapid carbonation.

This article is a PNAS Direct Submission.

[1]To whom correspondence should be addressed. E-mail: peterk@ldeo.columbia.edu.

*Gerdemann SJ, Dahlin DC, O'Connor WK, Penner LR, Second Annual Conference on Carbon Sequestration, Alexandria, VA, May 5–8, 2003. Report no. DOE/ARC-2003-018, OSTI ID: 898299 8 pp.

This article contains supporting information online at www.pnas.org/cgi/content/full/0805794105/DCSupplemental.

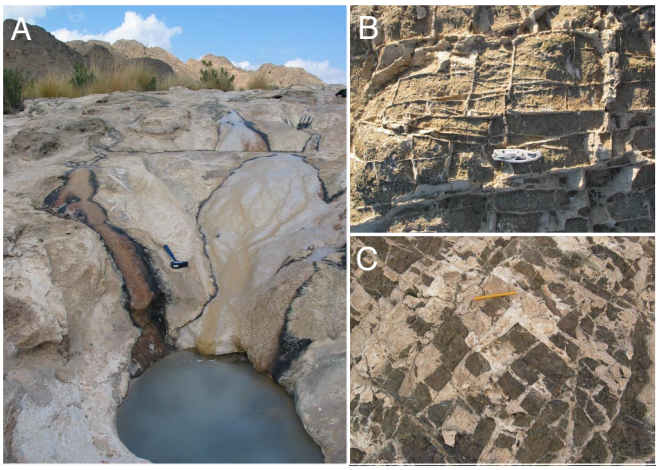

Fig. 1. Photographs of travertine and carbonate veins in Oman. (*A*) Actively depositing travertine near the village of Falaij (22.846°N, 58.056°E) with rock hammer for scale, altered peridotite in the background. (*B*) White carbonate veins weathering out in positive relief in altered peridotite at ''Duck'' (22.815°N, 58.838°E) with pocket knife for scale. (*C*) White carbonate veins in altered peridotite north of the village of Batin (22.925°N, 58.671°E) with pencil for scale.

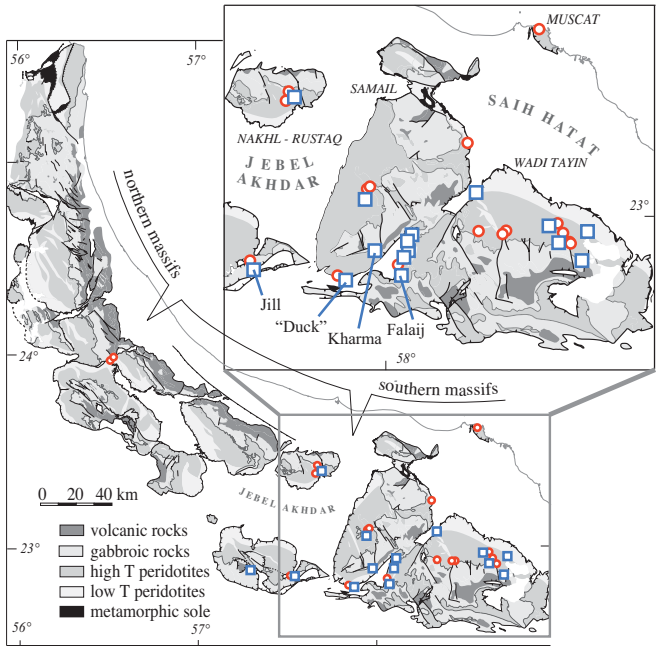

Fig. 2. Geologic map of the Oman ophiolite (8), with locations of carbonate samples dated by using ^{14}C (red circles, Table S1) and locations of known travertine deposits in the Bahla, Samail, and Wadi Tayin ophiolite massifs [blue squares; for perimeter maps of the ''Duck,'' Kharma and Falaij travertines, see Fig. S1; for more information on the Jill travertine deposit, see Clark and Fontes (28)]. Based on our observations of these 3 southernmost massifs, we infer that there are at least 45 similar travertine deposits in the entire ophiolite. We only show locations of travertine deposits that we have personally observed, and there are probably many more even in the southern massifs. In addition to travertine deposits on the surface (Fig. 1*A*, with locations shown here), there are thick travertine deposits forming within alluvial and gravel terraces (examples in Fig. 4).

Evidence for natural, low-temperature hydration and carbonation of mantle peridotite can be found in springs and associated travertines in catchments composed of mantle peridotite (12–19), and in outcrops of altered peridotite with abundant carbonate veins (e.g., refs. 20–26). High alkalinity, stable isotope ratios, and formation of travertine and carbonate cemented conglomerates in springs (Fig. 1*A*) indicate ongoing serpentinization involving meteoric water at low temperature. In addition to travertine at springs, carbonate veins are also found within host peridotite (Fig. 1 *B* and *C*).

Vein and travertine formation are linked (e.g., refs. 15–19). Groundwater reacting with peridotite in near-surface, open systems forms water rich in Mg and HCO_3^-, which we call *Type 1* waters, according to Barnes and O'Neil (18). When these waters become isolated from the atmosphere, continued reaction with peridotite leads to precipitation of abundant magnesite and dolomite as veins; the resulting waters become progressively richer in Ca and OH^-, and impoverished in dissolved carbon, approaching a pH of 12. When these Ca-OH^--rich, carbon-poor, *Type 2* waters emerge near the surface, to mix with Mg-HCO_3^- waters or react with the atmosphere, they precipitate abundant calcite and dolomite in near-surface veins, carbonate cement in unconsolidated sediment, and travertine.

Rate of Peridotite Carbonation in the Samail Ophiolite, Oman

The rate of CO_2 uptake via weathering of peridotite is poorly known. We sampled solid carbonate forming from peridotite over a wide area in the Samail ophiolite [Fig. 2 and supporting information (SI) Table S1], including veins from ridges far from present day springs as well as currently forming travertine. Previous workers inferred that most veins far from present-day springs are 30–90 million years old, related to formation of oceanic crust, emplacement of the ophiolite, and Eocene extension (e.g., refs. 15, 21, 22, 27). However, all of our samples have ^{14}C ages from 1,600 to 43,000 years, similar to the previously measured range of 840 to 36,000 years in the vicinity of a single, actively forming travertine in Oman (28). Samples of veins from ridges are mainly composed of dolomite and magnesite. In general, they are somewhat older than calcite-rich travertine and calcite-dolomite veins near active springs. However, the vein samples have an average age of ≈26,000 years, with a fairly ''flat'' age distribution (Fig. 3), and none are too old to date with ^{14}C.

The observed volume of carbonate terraces and veins in the Samail ophiolite, together with their ages, can be used to estimate the rate of CO_2 uptake via formation of solid carbonate

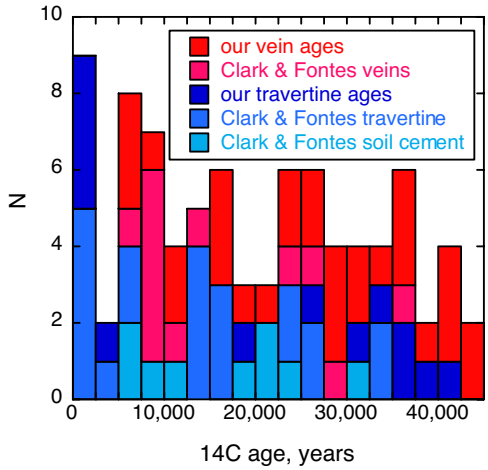

Fig. 3. Combined histogram of ^{14}C ages for our samples (Fig. 2, Table S1) and those of Clark and Fontes (28). The Clark and Fontes samples were taken from a single actively forming travertine deposit near the village of Jill, and carbonate veins in the underlying peridotite within a few meters of the travertine.

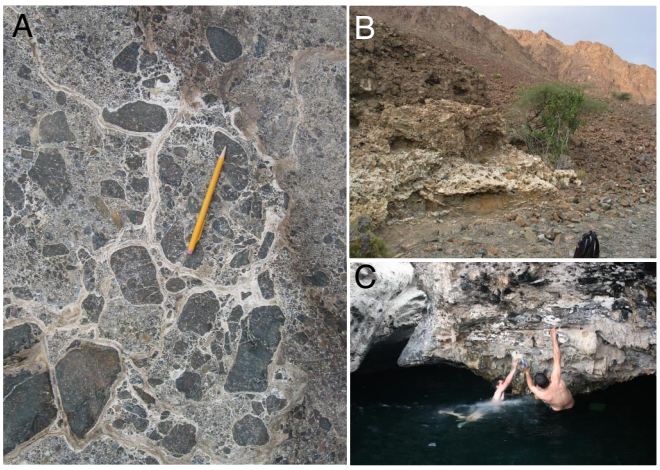

Fig. 4. Carbonate veins and massive travertine ''inflating'' carbonate-cemented, peridotite cobble conglomerate (*A*; 22.9845°N, 58.6322°E) and young alluvial fan deposits (*B*; 22.902°N, 58.371°E). Sampling stalactites forming beneath overhang in peridotite cobble conglomerate (*C*; 22.9875°N, 22.6327°E).

minerals in 2 ways. First, we can estimate the mass of veins directly, and divide this by their average age. Poupeau *et al.* (29) estimated an erosional denudation rate of ≈0.3 mm/yr for northern Oman. The ages of carbonate veins in peridotite suggest that veins form mainly in a thin weathering horizon that keeps pace with erosion; this horizon must generally be ≈15 m thick (erosion rate ≈0.0003 m/yr · maximum age of carbonate veins ≈50,000 years). Newly created road cuts in Oman peridotites reveal abundant, submillimeter carbonate veins on joint surfaces. We measured the vein abundance as ≈1 vol% in transects along road cuts (Table S2); 1% of the volume of a 15-m-thick weathering horizon in the Oman peridotite corresponds to $\approx 10^{12}$ kg of CO_2, for an average CO_2 uptake of $\approx 4 \cdot 10^7$ kg/yr.

We can independently estimate the mass of travertine formed at and near the surface by alkaline springs, and infer the associated mass of carbonate veins far from the surface that must be formed during recharge of these springs. Based on our relatively detailed, although incomplete, mapping in the southern third of the ophiolite, we estimate that there are ≈45 travertine terraces in the Samail ophiolite (Fig. 2) that are ≈1 m thick, with exposed areas ≈200,000 m^2 (Fig. S1), comprising a total of $\approx 10^7$ m^3 of exposed travertine. Travertine extends beneath alluvium downslope from outcrop areas, and travertine deposits are underlain by a zone ≈10 m thick with ≈5% calcite-rich veins (Table S2), so that their total volume is probably ≈2.5 times the exposed volume. Near-surface deposits, similar in composition and age to the travertine terraces, occur as massive carbonate bands, veins, and cement in alluvial terraces and conglomerates with peridotite clasts (Fig. 4). The volume of carbonate cement derived from Ca-OH^- waters in peridotite sediments is hard to estimate, but is at least as large as the volume of travertine terraces. All of these factors, taken together, suggest that the volume of near-surface travertine and carbonate in peridotite sediments in Oman is $\approx 5.5 \cdot 10^7$ m^3 or more, corresponding to at least $\approx 10^{11}$ kg of CO_2.

Spring waters and shallow groundwater in peridotite catchments fall into 2 compositional groups, as discussed above and illustrated in Fig. S2. We can estimate carbonation rates from water compositions, assuming (*i*) all carbon in type 1 waters is consumed to form solid carbonate during formation of type 2 waters, and (*ii*) the difference in Ca between type 2 and type 1 waters is precipitated as calcite when type 2 waters reach the surface. In California, type 1 waters have ≈0.2 mmol of Ca per liter, and up to 24 mmol of carbon per liter (19). Type 2 waters have essentially no carbon, and ≈1.5 mmol Ca per liter (Fig. S2). Thus, for every mole of calcite near the surface, up to ≈24/(1.5–0.2) or 18 mol of magnesite form in the subsurface.

There is a maximum of ≈8 mmol/L, carbon in Oman Type 1 waters, lower than in California, whereas Ca concentration is ≈0.8 mmol/L, higher than in California. There is essentially no carbon, and ≈1.6 mmol Ca in type 2 waters in Oman. It is not clear whether these values reflect lower carbon concentrations in Oman waters compared with those in California, or whether end-member type 1 waters in Oman have not yet been sampled. If, for every mole of near-surface calcite, 8/(1.6–0.8) or 10 mol of magnesite are precipitated as veins, this yields $\approx 10^{12}$ kg of CO_2 in veins, consistent with the estimate derived from measured vein abundance and the inferred thickness of the veined horizon.

In summary, estimates of the volume of carbonate deposits formed during ongoing weathering of peridotite, and their average age of 26,000 years, indicate that $\approx 4 \cdot 10^7$ kg of atmospheric CO_2 per year are consumed via mineral carbonation in the Samail ophiolite, or ≈2 tons/km^3 of peridotite. This strikingly rapid rate is compared with CO_2 flux in rainwater and groundwater, and discussed further in the *SI Text*. Here, we emphasize that a factor of 100,000 increase in this rate could consume 4 billion tons of CO_2 per year, ≈10% of the annual increase in atmospheric CO_2 because of anthropogenic emissions, via carbonation of peridotite in Oman.

Enhancing Rates of Peridotite Carbonation in Situ

In this section, we propose and evaluate ways to increase CO_2 uptake in situ in tectonically exposed peridotite massifs. In the Samail ophiolite and other large massifs, an obvious approach is to increase the depth of the weathering horizon by a factor of 200, from ≈15 m to ≈3 km in the peridotite via drilling and hydraulic fracture (30). Additional fracture may be anticipated as a result of thermal expansion during heating (31), volume increase during hydration (32–34), and volume increase during carbonation. Carbonation of olivine (Eq. **2b**) results in ≈44% increase in the solid volume, which can lead to enormous stresses that may be relieved by cracking and additional expansion (Fig. 1 *B* and *C*).

An additional increase in the carbonation rate, by a factor of $> \approx 10^6$, could be achieved by raising the temperature of the peridotite and injecting CO_2-rich fluids. There is an optimal temperature for peridotite carbonation. Heating from low temperature speeds the diffusive kinetics of hydration and carbonation. However, the chemical potential driving the reaction is reduced as the temperature approaches the equilibrium phase boundary for serpentine or carbonate mineral stability. The combined effect yields a maximum reaction rate at a temperature intermediate between surface conditions and the equilibrium phase boundary (Fig. S3). The reaction rate for serpentinization as a function of temperature has a maximum value at ≈260 °C over a range of pressure (35), whereas the rate of carbonation is optimized at, for example, 185 °C and 150 bars CO_2 pressure.* We fit data on rates of serpentinization of olivine with grain size 58–79 μm (35) and carbonation of olivine with grain size ≤75 μm* as a function of temperature and CO_2 partial pressure, yielding a serpentinization rate (Fig. S4)

$$\Gamma = 0.00000100 \exp[-0.000209(T - 260°C)^2] \quad \textbf{[3]}$$

and a carbonation rate (Fig. S5 and Fig. S6).

$$\Gamma \sim 1.15 \cdot 10^{-5} (P(CO_2), \text{bars})^{1/2} \exp[-0.000334(T - 185°C)^2] \quad \textbf{[4]}$$

GEOLOGY

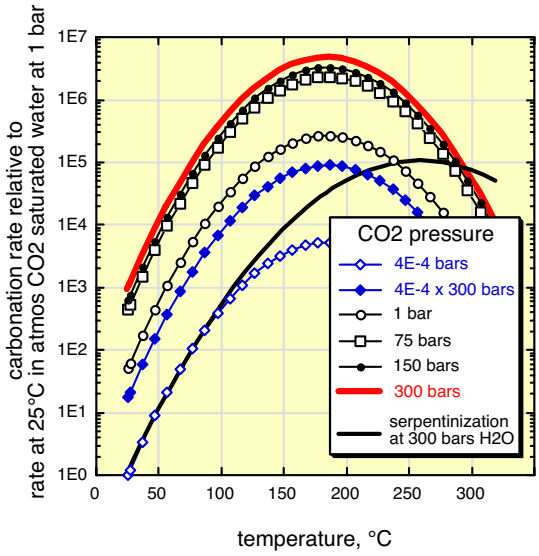

Fig. 5. Rates of olivine carbonation (lines and symbols) and serpentinization (black line, no symbols) as a function of temperature and pressure, compared with the rates at 25 °C for surface water equilibrated with the atmosphere at 1 bar. A range of curves are shown for carbonation, with a single curve for serpentinization of olivine saturated in aqueous fluid at 300 bars. Note that the reaction rate for carbonation is much higher than that for serpentinization at 300 bars and temperature $< \approx 250$ °C. The enthalpy change, per kilogram, is also ≈3 times larger for carbonation than for serpentinization (see text).

both in units of mass fraction per second. Heating and raising the partial pressure of CO_2 can increase the carbonation rate by a factor of $>10^6$ (Fig. 5), and with the potential for increasing the thickness of the weathering horizon by fracturing, the overall increase could be a factor of $\approx 10^9$. Together with the estimated present-day CO_2 uptake at the end of the previous section, this corresponds to $2 \cdot 10^9$ tons/km^3 per year.

Thermal Effects of Advection, Diffusion, and Reaction

The change in temperature for a particular volume in a subsurface, porous aquifer can be approximated in 1 dimension as

$$dT/dt = (T_{in} - T)\rho_f C_p^f \phi w/(\rho_s C_p^s d) - (T - T_o)\kappa/d^2 + \Gamma(T) A \Delta H/[C_p^s(1 - \phi) + C_p^f(\phi)] \quad [5]$$

where T_{in} is the temperature of incoming water or aqueous fluid (°C or Kelvin), T is the current temperature in the volume, T_o is the far-field temperature, outside the volume, which is equal to the initial temperature in the volume, ρ_f and ρ_s are the densities of the fluid and solid, C_p^f and C_p^s are the heat capacities of the fluid and solid, ϕ is the porosity or volume fraction of fluid (nondimensional, 1% in all calculations shown here), w is the fluid flow velocity (m/s), d is the dimension or "size" of the volume (m, 1,000 m in all calculations shown here), κ is the thermal diffusivity (10^{-6} m^2/s), Γ is the reaction rate, which is a function of temperature (units of 1/s), A is the fraction of the rock available for reaction in the volume (nondimensional), and ΔH is the enthalpy change due to reaction. The use of a reactive volume fraction term <1 accounts for the fact that most natural rocks do not have an effective grain size of ≈70 μm, unlike the experiments used to calibrate Eqs. **3** and **4**. The volume available for reaction is product of a diffusion distance times the surface area of grains. The surface area is proportional to the radius squared, so the use of a reactive volume fraction of 0.01% corresponds to modeling of an effective "grain size" or fracture spacing of ≈7 mm, 100 times larger than in the experiments.

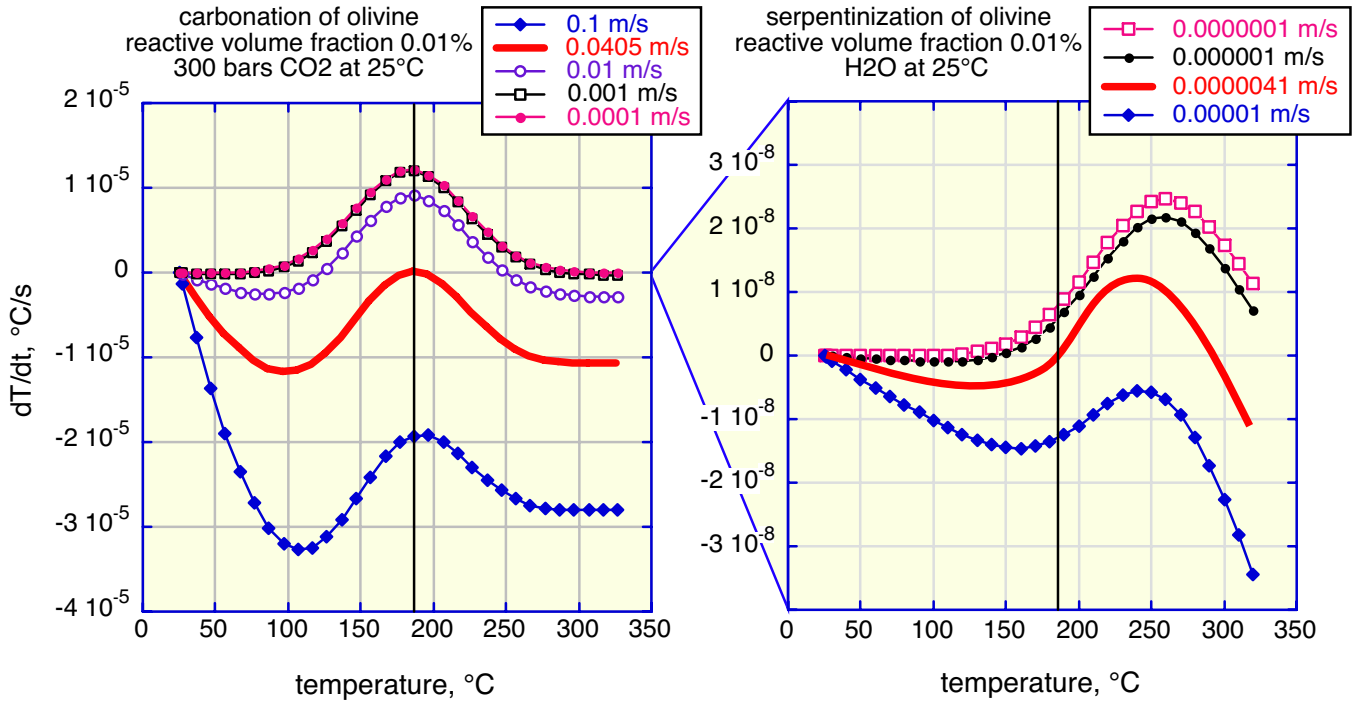

Fig. 6. Calculated rate of change of temperature due to olivine carbonation (*Left*) and serpentinization (*Right*) at 300 bars as a function of rock temperature and fluid flow rate, for 25 °C fluid and a reactive volume fraction of 0.01%, from our 1-dimensional energy balance model (Eq. **5**). A constant rock temperature of 185 °C can be maintained by pumping 25 °C CO_2 at ≈0.040 m/s, or by pumping 25 °C H_2O at $\approx 4.1 \cdot 10^{-6}$ m/s. Note that the range of temperature derivatives and steady-state flow rates at 185 °C are much larger for the olivine carbonation reaction than for serpentinization.

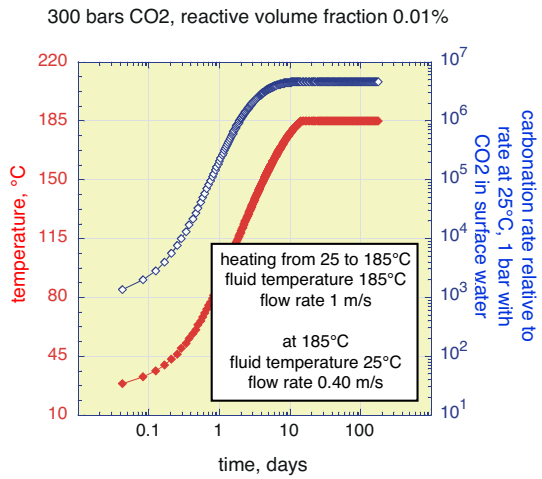

Fig. 7. Calculated temperature and carbonation rate, relative to the rate at 25 °C for CO_2 in surface water at equilibrated with the atmosphere at 1 bar, for a 3-step method beginning with drilling and hydraulic fracture, followed by heating via rapid pumping of 185 °C CO_2, followed by slower pumping of 25 °C CO_2 to maintain constant temperature.

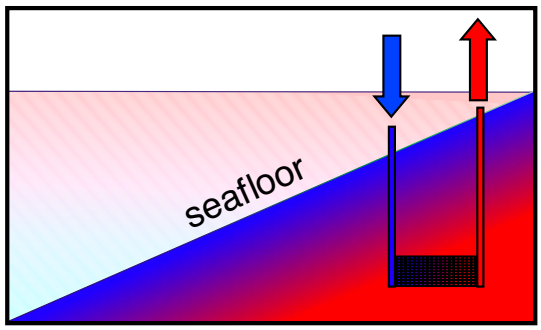

Fig. 8. Schematic representation of 2 bore holes into peridotite below the seafloor, connected by a fracture network. Color gradients below the seafloor represent temperature variation with blue indicative of ≈0–25 °C and red indicative of ≈150 °C. As a result of thermal convection, near-surface seawater would descend one hole (with a controlled flux) and rise through the other. At depth, the water would be heated by the geothermal gradient and by exothermic serpentinization and carbonation reactions. Mineral carbonation in the peridotite would consume dissolved CO_2 from evolving seawater along the flow path.

For these calculations, densities, heat capacities, and enthalpies were obtained from standard references reviewed and updated by Gottschalk (36) and similar data from the National Institute of Standards (NIST) Chemistry WebBook (NIST Standard Reference Database Number 69, June 2005 Release) at http://webbook.nist.gov/chemistry/. For our calculations, we fit simple functions to the temperature dependence of thermodynamic properties from 25 to 300 °C. For H_2O and CO_2, we used 300 bars pressure for the calculations discussed in this section. Above 300 °C, and far from this pressure, our calculations would be inaccurate.

Fig. 6 illustrates results from Eq. **5** in terms of temperature change, dT/dt, versus initial temperature, for fluid porosity of 0.01 (1%), fluid temperature of 25 °C at 300 bars pressure, with reactive volume fraction A of 0.01%. At high flow rates with cold (25 °C) fluid, the volume cannot be heated by exothermic reactions. At low flow rates, advective cooling is negligible, and temperature is controlled by exothermic heating and diffusive cooling. To optimize olivine carbonation rates, fluid flow should be adjusted to yield $dT/dt = 0$ at ≈185 °C. Heating due to hydration (serpentinization) is less effective than heating due to carbonation. This is partly because, for example, at1 bar and 25 °C, ΔH is ≈250 kJ/kg for serpentinization (Eq. **1**), whereas carbonation (Eq. **2**) evolves ≈760 kJ/kg, and partly because serpentinization is slower than carbonation for temperatures between 25 and 185 °C (Fig. 5).

Recipes for in Situ Carbonation of Peridotite

One approach is to take maximum advantage of the exothermic heat output available from the carbonation reaction, by raising a rock volume to the optimal temperature for peridotite carbonation. To reach and maintain 185 °C, it is necessary to preheat the rock volume. This can be achieved via a variety of flow rates, fluid temperatures, and fluid compositions. Initial heating should probably be via high flow rates by using preheated fluids. Later, because large volumes of rock are to be held at 185 °C to optimize CO_2 uptake, output fluid can be used to heat other areas. This may happen spontaneously as hot fluid flows into colder, surrounding rock.

Because pumping rates for 25 °C fluid must remain low to maintain high temperature, dissolved CO_2 in surface water cannot be supplied rapidly enough to keep pace with the enhanced carbonation rates modeled here. Instead, injection of pure CO_2, or a CO_2-rich fluid mixture, is required to keep pace with the enhanced reaction rate. As seen in Fig. 6, dT/dt resulting from carbonation is zero at 185 °C when the flow rate of pure CO_2 injected at 300 bars and 25 °C is ≈0.040 m/s and the reactive volume fraction is 0.01%. At these conditions, our 1-dimensional model delivers ≈0.166 kg of CO_2 per s to a $1 \times 1 \times 1000$ m^3 rock volume, and consumes ≈0.127 kg of CO_2 per s to form solid magnesite. All olivine is consumed after ≈190 days, consuming ≈2,000 tons of CO_2 per 1,000 m^3, or—scaling up—$2 \cdot 10^9$ tons of CO_2 per km^3 at ≈$4 \cdot 10^9$ tons/yr. Note that this is an *independent estimate* of CO_2 uptake, which is consistent with the rate of ≈$2 \cdot 10^9$ tons/km^3 per year derived at the end of the section entitled *Enhancing Rates of Peridotite Carbonation in Situ*.

Fig. 7 provides an example of a 3-step process, with drilling and hydrofracture of peridotite at depth, followed by injection of hot fluid to heat the newly fractured peridotite to 185 °C, followed in turn by injection of pure CO_2 at 25 °C to sequester carbon whereas exothermic carbonation maintains the system at 185 °C. Our simple calculations show that a factor of more than 1 million enhancement in the carbonation rate is achievable. Note that we have not incorporated the "cost-free" heating afforded by the geothermal gradient; if northern Oman lies along a typical continental geotherm of 10–20 °C/km (37), then the initial temperature at the bottom of a 3-km drill hole will be 55–85 °C, not the initial 25 °C used in our model. Indeed, Neal and Stanger (15) report that alkaline springs in Oman peridotites have temperatures up to 15 °C hotter than normal groundwater in the same locations, and infer that the alkaline waters have been heated during circulation at depths of 700 m or more.

Our calculations are done assuming that the reactive volume fraction is constant, whereas, in practice, reactive surfaces may become depleted. It may be necessary to reduce the fluid flow rate as this occurs, to avoid cooling the reacting volume. At some point, in particular, if reaction-driven cracking does not occur, it may be necessary to hydraulically fracture the system again to expose additional reactive surface area. More optimistically, temperature change and the large increases in solid volume due to mineral hydration and carbonation will cause cracking and increased permeability. In any case, eventually all accessible olivine in a given rock volume will be depleted. Before this occurs, fluid heated by reaction in 1 region can be pumped into an adjacent area to begin the process anew.

An alternative process could avoid prolonged pumping of fluid and use of purified CO_2. In Oman, New Caledonia, and Papua New Guinea, peridotite is present beneath a thin veneer

of sediment offshore. Here, peridotite could be drilled and fractured, and a volume could be heated. Again, little heating would be required if, for example, the initial temperature at the bottom of a 5-km bore hole is 100 °C (Fig. 8). Then, controlled convection of near-surface water through the rock volume could sustain high temperature via exothermic hydration of olivine at a flow rate of $\approx 4{\cdot}10^{-6}$ m/s (as seen in Fig. 3 *Right*). The carbonation rate would be limited by supply of dissolved CO_2 in convecting seawater—only $\approx 10^4$ tons of CO_2 per km^3 of peridotite per year at a flow rate of $4{\cdot}10^{-6}$ m/s—but the cost would be relatively low.

Conclusion: Promising Alternatives to ex Situ Mineral Carbonation

Because these proposed methods of in situ mineral carbonation use the chemical potential energy inherent in tectonic exposure of mantle peridotite at the Earth's surface, the optimal temperature for carbonation can be maintained in a rock volume at little expense. Further, rock volumes at depth are, inherently, at relatively high pressure and elevated temperature. Thus, compared with engineered, mineral carbonation "at the smokestack," this method does not involve quarrying and transportation of peridotite, processing of solid reactants via grinding and heat treatment, or maintaining high temperature and pressure in a reaction vessel. Instead, the major energy investments in this method would be for drilling, hydraulic fracturing, pumping fluid, preheating fluid for the first heating step, and purification of CO_2. Also, unlike ex situ mineral carbonation, this method may require on-site CO_2 capture or transport of purified CO_2 to the in situ carbonation locality.

Clearly, more elaborate models combined with field tests will be required to evaluate and optimize this method. For example, it is difficult to predict the consequences of hydraulic fracturing of peridotite, plus cracking associated with heating, hydration, and carbonation, in terms of permeability and reactive volume fraction. Such processes are all-but-impossible to simulate in the laboratory. Large-scale field tests should be conducted, because the proposed method of enhanced natural CO_2 sequestration provides a promising potential alternative to storage of supercritical CO_2 fluid in underground pore space, and to engineered, ex situ mineral carbonation.

ACKNOWLEDGMENTS. We thank everyone at the Geological Survey of Oman and the Directorate General of Minerals in the Ministry of Commerce and Industry, Sultanate of Oman, for their generosity, particularly, Hilal Al Azri, Ali Al Rajhi, and Salim Al Busaidi. We thank many friends, especially Karen Benedetto, Martin Collier, Brad Hacker, Karen Hanghøj, Greg Hirth, Sam Krevor, John Rudge, and Lisa Streit for help during the 2007 and 2008 Oman field seasons; Hacker, Hirth, Rudge, Wally Broecker, Mark Ghiorso, Al Hofmann, and Marc Spiegelman for scientific discussions and advice; Benedetto, Hanghøj, Streit, Bill Curry, Kathy Elder, Al Gagnon, Susan Handwork, Rindy Osterman, and Margaret Sulanowska for assistance with (ongoing) sample preparation and analysis; Mike Purdy and David Hirsh for moral and financial support; Dave Walker for editorial advice; and Greg Dipple and an anonymous reviewer for helpful suggestions. This work was supported by a Columbia Research Initiative in Science and Engineering Grant (to P.B.K. and J.M.).

1. Metz B, Davidson O, de Coninck H, Loos M, Meyer L, eds (2005) *IPCC Special Report on Carbon Dioxide Capture and Storage* (Cambridge Univ Press, New York), p 431.
2. Seifritz W (1990) CO2 disposal by means of silicates. *Nature* 345:486.
3. Lackner KS, Wendt CH, Butt DP, Joyce EL, Sharp DH (1995) Carbon dioxide disposal in carbonate minerals. *Energy* 20:1153–1170.
4. Lackner KS, Butt DP, Wendt CH (1997) Progress on binding CO2 in mineral substrates. *Energy Convers Manage* 38:S259–S264.
5. Mazzotti M, *et al.* (2005) Mineral carbonation and industrial uses of CO2. *IPCC Special Report on Carbon Dioxide Capture and Storage*, eds Metz B, Davidson O, de Coninck H, Loos M, Meyer L (Cambridge Univ Press, Cambridge, UK), pp 319–338.
6. Solomon S, *et al.* (2007) Technical summary. *Climate Change 2007*: *The Physical Science Basis. Contribution of Working Group I to the Fourth Assessment Report of the Intergovernmental Panel on Climate Change*, eds Solomon S, *et al.* (Cambridge Univ Press, Cambridge, UK), pp 20–91.
7. Nicolas A, Boudier E, Ildefonse B, Ball E (2000) Accretion of Oman and United Arab Emirates ophiolite: Discussion of a new structural map. *Marine Geophys Res* 21(3–4):147–179.
8. Fyfe WS (1974) Heats of chemical reactions and submarine heat production. *Geophys J Roy Astr Soc* 37(1):213–215.
9. Kelley DS, *et al.* (2001) An off-axis hydrothermal vent field near the Mid-Atlantic Ridge at 30 degrees N. *Nature* 412(6843):145–149.
10. Emmanuel S, Berkowitz B (2006) Suppression and stimulation of seafloor hydrothermal convection by exothermic mineral hydration. *Earth Planet Sci Lett* 243(3–4):657–668.
11. Allen DE, Seyfried WE (2004) Serpentinization and heat generation: Constraints from Lost City and Rainbow hydrothermal systems. *Geochim Cosmochim Acta* 68(6):1347–1354.
12. Zedef V, Russell MJ, Fallick AE, Hall AJ (2000) Genesis of vein stockwork and sedimentary magnesite and hydromagnesite deposits in the ultramafic terranes of southwestern Turkey: A stable isotope study. *Econ Geol* 95(2):429–445.
13. Wenner DB, Taylor HPJ (1974) D/H and 18O/16O studies of serpentinization of ultramafic rocks. *Geochim Cosmochim Acta* 38:1255–1286.
14. Weyhenmeyer CE (2000) Origin and evolution of groundwater in the alluvial aquifer of the Eastern Batinah Coastal Plain, Sultanate of Oman. PhD thesis (Geologisches Institut, Universität Bern), 202 pp.
15. Neal C, Stanger G (1985) Past and present serpentinization of ultramafic rocks: An example from the Semail ophiolite nappe of northern Oman. *The Chemistry of Weathering*, ed Drewer JI (D. Reidel Publishing Company, Dordrecht, Holland), pp 249–275.
16. Cipolli F, Gambardella B, Marini L, Ottonello G, Zuccolini MV (2004) Geochemistry of high-pH waters from serpentinites of the Gruppo di Voltri (Genova, Italy) and reaction path modeling of CO2 sequestration in serpentinite aquifers. *Appl Geochem* 19(5):787–802.
17. Bruni J, *et al.* (2002) Irreversible water-rock mass transfer accompanying the generation of the neutral, Mg-HCO3 and high-pH, Ca-OH spring waters of the Genova province, Italy. *Appl Geochem* 17(4):455–474.
18. Barnes I, O'Neil JR (1969) Relationship between fluids in some fresh alpine-type ultramafics and possible modern serpentinization, western United States. *GSA Bull* 80(10):1947–1960.
19. Barnes I, LaMarche VC, Himmelberg G (1967) Geochemical evidence of present-day serpentinization. *Science* 156(3776):830–832.
20. Hansen LD, Dipple GM, Gordon TM, Kellett DA (2005) Carbonated serpentinite (listwanite) at Atlin, British Columbia: A geological analogue to carbon dioxide sequestration. *Can Mineral* 43:225–239.
21. Nasir S, *et al.* (2007) Mineralogical and geochemical characterization of listwaenite from the Semail ophiolite, Oman. *Chemie Der Erde* 67:213–228.
22. Wilde A, Simpson L, Hanna S (2002) Preliminary study of Cenozoic alteration and platinum deposition in the Oman ophiolite. *J Virtual Explorer* 6:7–13.
23. Früh-Green G, Weissert H, Bernoulli D (1990) A multiple fluid history recorded in Alpine ophiolites. *J Geol Soc London* 147:959–970.
24. Trommsdorff V, Evans B, Pfeifer HR (1980) Ophicarbonate rocks: Metamorphic reactions and possible origin. *Arch Sci Genève* 33:3610364.
25. Naldrett AJ (1966) Talc-carbonate alteration of some serpentinized ultramafic rocks south of Timmins, Ontario. *J Petrol* 7:489–499.
26. Stanger G (1985) Silicified serpentinite in the Semail nappe of Oman. *Lithos* 18(1):13–22.
27. Python M, Ceuleneer G, Ishida Y, Barrat J-A, Arai S (2007) Oman diopsidites: A new lithology diagnostic of very high temperature circulation in mantle peridotite below oceanic spreading centers. *Earth Planet Sci Lett* 255:289–305.
28. Clark ID, Fontes JC (1990) Paleoclimatic reconstruction in northern Oman based on carbonates from hyperalkaline groundwaters. *Quat Res* 33(3):320–336.
29. Poupeau G, Saddiqi O, Michard A, Goffé B, Oberhänsli R (1998) Late thermal evolution of the Oman Mountains subophiolitic windows: Apatite fission-track thermochronology. *Geology* 26:1139–1142.
30. Valkó P, Economides MJ (1995) *Hydraulic Fracture Mechanics* (Wiley, Chichester), p 298.
31. Fredrich JT, Wong TF (1986) Micromechanics of thermally induced cracking in 3 crustal rocks. *J Geophys Res* 91:2743–2764.
32. Jamtveit B, Malthe-Sorenssen A, Kostenko O (2008) Reaction enhanced permeability during retrogressive metamorphism. *Earth Planet Sci Lett* 267:620–627.
33. Iyer K, Jamtveit B, Mathiesen J, Malthe-Sorenssen A, Feder J (2008) Reaction-assisted hierarchical fracturing during serpentinization. *Earth Planet Sci Lett* 267:503–516.
34. Fletcher RC, Buss HL, Brantley SL (2006) A spheroidal weathering model coupling porewater chemistry to soil thickness during steady-state denudation. *Earth Planet Sci Lett* 244:444–457.
35. Martin B, Fyfe WS (1970) Some experimental and theoretical observations on kinetics of hydration reactions with particular reference to serpentinization. *Chem Geol* 6(3):185–202.
36. Gottschalk M (1997) Internally consistent thermodynamic data for rock-forming minerals in the system SiO2-TiO2-Al2O3-Fe2O3-CaO-MgO-FeO-K2O-Na2O-H2O-CO2. *Eur J Mineral* 9:175–223.
37. Blackwell DD (1971) The thermal structure of the continental crust. *The Structure and Physical Properties of the Earth's Crust,* Geophysical Monograph 14, ed Heacock JG (American Geophysical Union, Washington, DC), pp 169–184.

Supporting Information

Kelemen and Matter 10.1073/pnas.0805794105

SI Text

Discussion of Rate of Magnesite and Dolomite Formation via Mineral Carbonation in Oman Peridotite. The rapid rate of formation of carbonate minerals via weathering of peridotite in Oman, consuming $\approx 4 \cdot 10^7$ kg of CO_2 per year, is striking for 2 reasons. First, it is faster than the influx of CO_2 dissolved in rainwater. Second, the veins are composed mainly of magnesite and dolomite, which are rare in Phanerozoic sedimentation.

Rainfall over the ophiolite ranges from 50 to 300 mm/yr (1, 2). The interannual variability is large, but this range is likely to have been roughly constant for most of the past 75,000 years with the exception of the "early Holocene humid period" from ≈9 to 8 ka (e.g., refs. 3 and 4). CO_2 concentration (all C as CO_2, for simplicity) is ≈1 ppm in rainwater over the ophiolite (5), yielding an annual flux of $\approx 1 \cdot 10^6$ kg of CO_2 from rainfall onto peridotite. Thus, even if all CO_2 in rainwater were consumed to form carbonate via peridotite weathering, this would be 40 times less than observed, estimated consumption of CO_2 via weathering.

In contrast, typical groundwater in the Oman ophiolite contains ≈200 ppm CO_2 (5) These are called type 1 waters in the main text, according to Barnes and O'Neil (6). Conversion of rainwater to groundwater takes place via near-surface weathering in an open system. As Mg and Ca concentrations in groundwater rise via water/rock reaction, this causes increased CO_2 uptake into the waters from the atmosphere (e.g., ref. 7). If all rainwater falling on the peridotite is modified to form typical groundwater, then precipitation of ≈20% of the CO_2 from groundwater—to form carbonate during continued, closed-system evolution of the groundwater to form type 2 alkaline spring water (7)—is required to explain the observed, estimated consumption of CO_2 via weathering.

Formation of strata-bound magnesite ($MgCO_3$) and dolomite ($Ca_{0.5}Mg_{0.5}CO_3$) in sedimentary sections was common early in Earth history, and is rare today, for reasons that continue to be the subject of active research, and this is known as the "Dolomite Problem" (8–11). There is a similar "Magnesite Problem" (12). Ca-Mg carbonate precipitation has recently been observed in highly reduced waters, where it is biologically catalyzed (13–20), including waters in weathering peridotite (21). It is possible that the unexpectedly rapid formation of magnesite and dolomite veins in peridotite of the Oman ophiolite is facilitated by microorganisms, and this should be an area of intensive future research, because these biological processes could perhaps be enhanced to facilitate CO_2 capture and storage.

However, it is not clear that the Dolomite Problem in understanding the kinetics of dolomite and magnesite formation within sedimentary sections extends to the formation of Mg-carbonate veins in peridotite, which may have been rapid and common throughout Earth history. We are not aware of any data on this topic. The kinetic experiments on olivine carbonation (Gerdemann SJ, Dahlin DC, O'Connor WK, Penner LR, Second Annual Conference on Carbon Sequestration, Alexandria, VA, May 5–8, 2003. Report no. DOE/ARC-2003-018, OSTI ID: 898299 8 pp) that underlie our model for enhanced in situ carbonation did not involve biologically catalyzed carbonation, and they yield rates that are approximately consistent with observed rates in Oman.

1. Babikir AAA (1985) On the distribution of rainfall over the Sultanate of Oman. *GeoJournal* 11:165–172.
2. Weyhenmeyer C, Burns SJ, Waber HN, Macumber PG, Matter A (2002) Isotope study of moisture sources, recharge areas, and groundwater flow paths within the eastern Batinah coastal plain, Sultanate of OMan. *Water Res J.* 38:1184, 1110.1029/2000WR000149.
3. Burns SJ, Fleitmann D, Matter A, Neff U, Mangini A (2001) Speleothem evidence from Oman for continental pluvial events during interglacial periods. *Geology* 29:623–626.
4. Fuchs M, Buerkert A (2008) A 20 ka sediment record from the Hajar Mountain range in N-Oman, and its implication for detecting arid–humid periods on the southeastern Arabian Peninsula. *Earth Planet Sci Lett* 265:546–558.
5. Matter JM (2005) Recharge areas and geochemical evolution of groundwater in an alluvial aquifer system in the Sultanate of Oman. *Hydrogeol J* 14:203–224.
6. Barnes I, O'Neil JR (1969) Relationship between fluids in some fresh alpine-type ultramafics and possible modern serpentinization, western United States. *GSA Bull* 80(10):1947–1960.
7. Bruni J, *et al.* (2002) Irreversible water-rock mass transfer accompanying the generation of the neutral, Mg-HCO3 and high-pH, Ca-OH spring waters of the Genova province, Italy. *Appl Geochem* 17(4):455–474.
8. Arvidson RS, Mackenzie FT (1999) The dolomite problem: Control of precipitation kinetics by temperature and saturation state. *Am J Sci* 299(4):257–288.
9. Holland HD, Zimmerman H (2000) The dolomite problem revisited. *Int Geol Rev* 42(6):481–490.
10. Burns SJ, McKenzie JA, Vasconcelos C (2000) Dolomite formation and biogeochemical cycles in the Phanerozoic. *Sedimentology* 47:49–61.
11. de Leeuw NH, Parker SC (2001) Surface-water interactions in the dolomite problem. *Phys Chem Chem Phys* 3(15):3217–3221.
12. Frank TD, Fielding CR (2003) Marine origin for Precambrian, carbonate-hosted magnesite? *Geology* 31:1101–1104.
13. Thompson JB, Ferris FG (1990) Cyanobacterial precipitation of gypsum, calcite, and magnesite from natural alkaline lake water. *Geology* 18:995–998.
14. van Lith Y, Warthmann R, Crisogono V, McKenzie JA (2003) Sulphate-reducing bacteria induce low-temperature Ca-dolomite and high Mg-calcite formation. *Geobiology* 1:71–79.
15. Vasconcelos C, McKenzie JA (1997) Microbial mediation of modern dolomite precipitation and diagenesis under anoxic conditions (Lagoa Vermelha, Rio de Janeiro, Brazil). *J Sed Res* 67(3):378–390.
16. Vasconcelos C, McKenzie JA, Bernasconi S, Grujic D, Tien AJ (1995) Microbial mediation as a possible mechanism for natural dolomite formation at low-temperatures. *Nature* 377(6546):220–222.
17. Warthmann R, van Lith Y, Vasconcelos C, McKenzie JA, Karpoff AM (2000) Bacterially induced dolomite precipitation in anoxic culture experiments. *Geology* 28:1091–1094.
18. Roberts JA, Bennett PC, Gonzalez LA, Macpherson GL, Milliken KL (2004) Microbial precipitation of dolomite in methanogenic groundwater. *Geology* 32:277–280.
19. Léveillé RJ, Longstaffe FJ, Fyfe WS (2007) An isotopic and geochemical study of carbonate-clay mineralization in basaltic caves: Abiotic versus microbial processes. *Geobiology* 5:235–249.
20. Léveillé RJ, Fyfe WS, Longstaffe FJ (2000) Geomicrobiology of carbonate-silicate microbialites from Hawaiian basaltic sea caves. *Chem Geol* 169:339–355.
21. Power IM, Wilson SA, Thom JM, Dipple GM, Southam G (2007) Biologically induced mineralization of dypingite by cyanobacteria from an alkaline wetland near Atlin, British Columbia, Canada. *Geochem Trans,* 10.1186/1467-4866-1188-1113.
22. Barnes I, O'Neil JR (1969) Relationship between fluids in some fresh alpine-type ultramafics and possible modern serpentinization, western United States. *GSA Bull* 80(10):1947–1960.
23. Barnes I, LaMarche VC, Himmelberg G (1967) Geochemical evidence of present-day serpentinization. *Science* 156(3776):830–832.
24. Barnes I, O'Neil JR, Trescases JJ (1978) Present day serpentinization in New-Caledonia, Oman and Yugoslavia. *Geochim Cosmochim Acta* 42(1):144–145.s
25. Cipolli F, Gambardella B, Marini L, Ottonello G, Zuccolini MV (2004) Geochemistry of high-pH waters from serpentinites of the Gruppo di Voltri (Genova, Italy) and reaction path modeling of CO2 sequestration in serpentinite aquifers. *Appl Geochem* 19(5):787–802.
26. Matter JM (2001) Geochemical evolution and hydrodynamics of groundwaters in the alluvial aquifer of the Dakhiliya Area, Sultanate of Oman. PhD thesis (Eidgenössische Technische Hochschule Zürich).
27. Matter JM (2005) Recharge areas and geochemical evolution of groundwater in an alluvial aquifer system in the Sultanate of Oman. *Hydrogeol J* 14:203–224.
28. Bruni J, *et al.* (2002) Irreversible water-rock mass transfer accompanying the generation of the neutral, Mg-HCO3 and high-pH, Ca-OH spring waters of the Genova province, Italy. *Appl Geochem* 17(4):455–474.
29. Martin B, Fyfe WS (1970) Some experimental and theoretical observations on kinetics of hydration reactions with particular reference to serpentinization. *Chem Geol* 6(3):185–202.

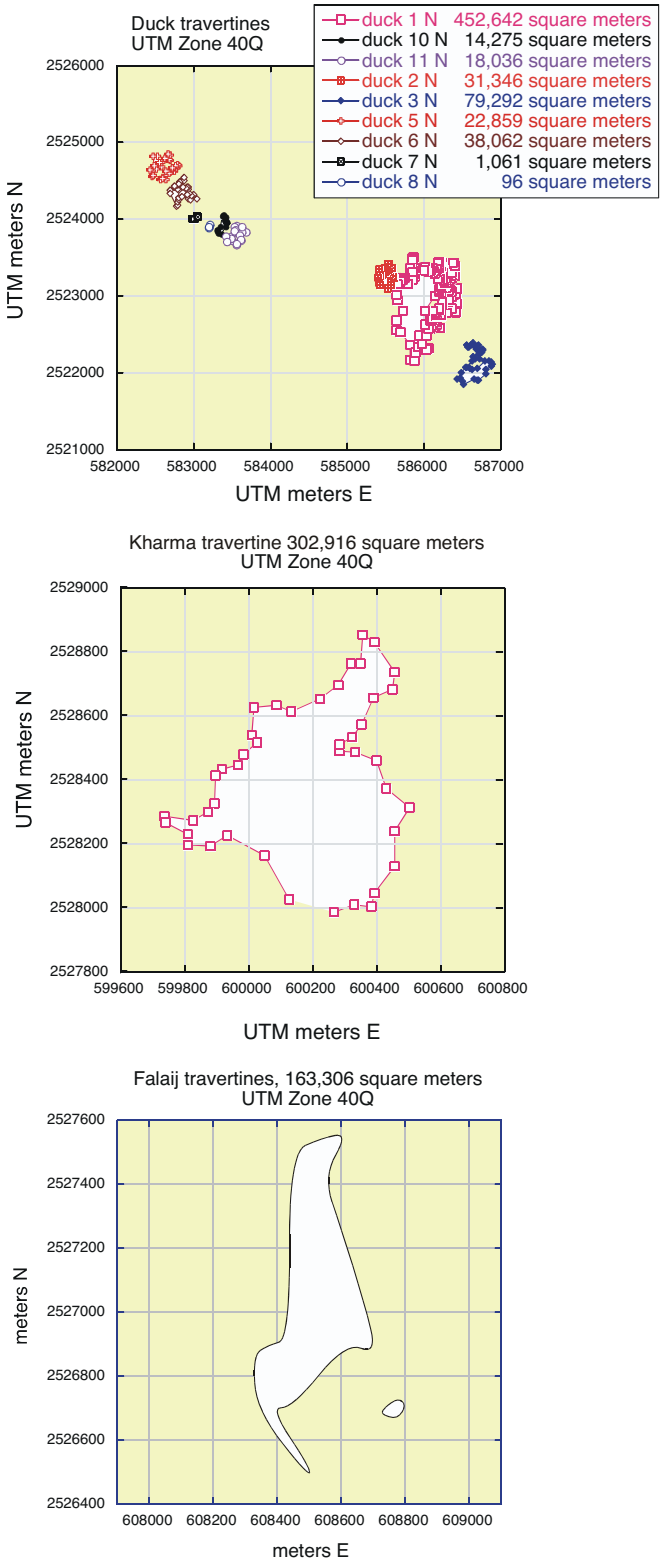

Fig. S1. Perimeter maps of travertine terraces at ''Duck,'' Kharma and Falaij localities, with estimated areas, with UTM coordinates in zone 40Q by using the WGS 84 datum. Note that the perimeter maps substantially underestimate the total area because travertine terraces continue beneath alluvial terraces downslope in most cases. For example, intermittent outcrops indicate an almost continuous layer of actively forming travertine beneath alluvial gravel that extends >10 km from ≈0608300 E, 2526500 N (south of the village of Falaij, see map in this figure) north to ≈0610250 E, 2536700 N. Also see Fig. 2.

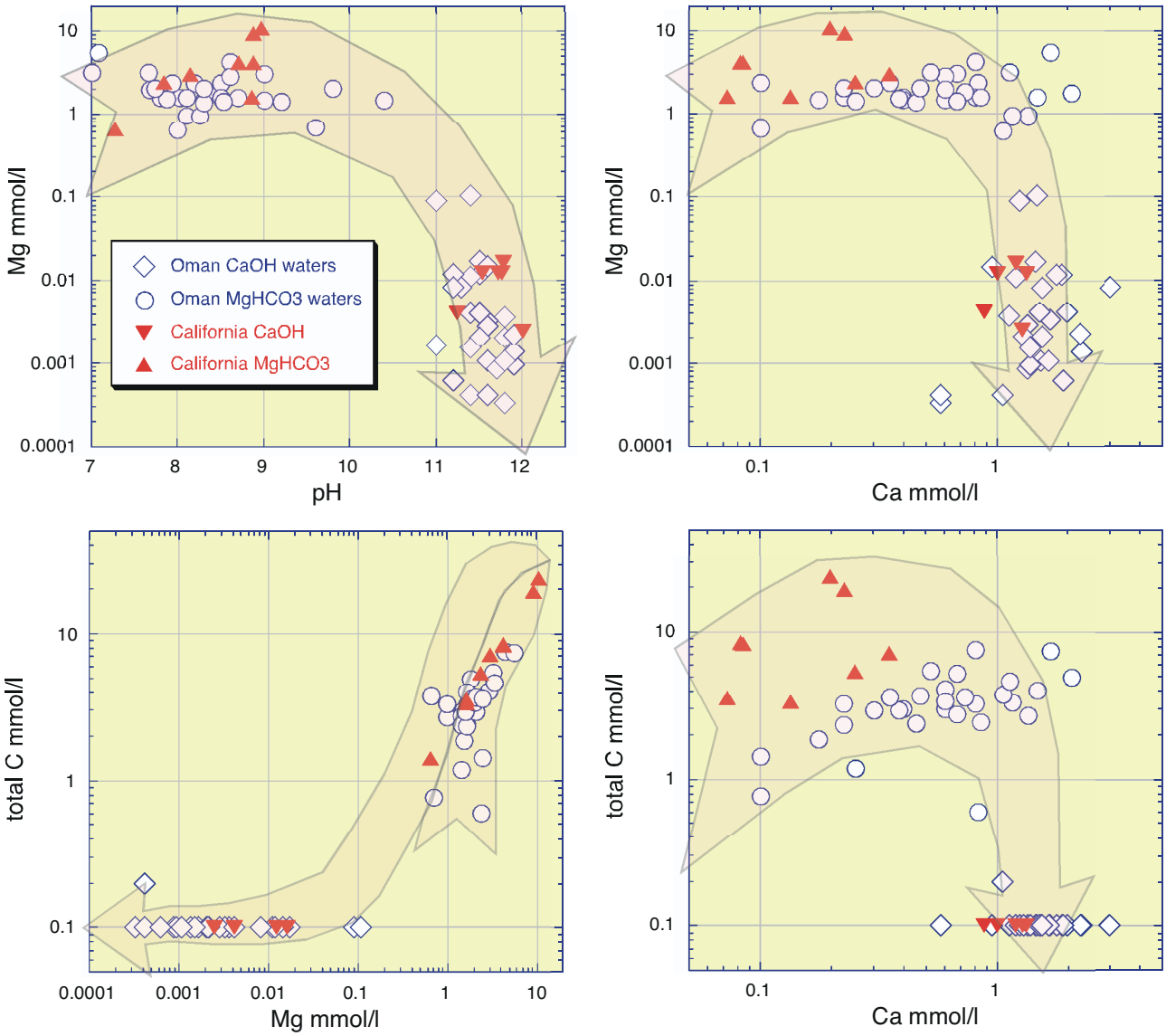

Fig. S2. Shallow ground water and spring water compositions from peridotite catchments in California (22–24) and Oman (25–27). All concentrations in mmol/liter. Light arrows show reaction path modeled by Bruni *et al.* (28) in which Mg and HCO_3^--rich, neutral waters are produced by open-system reaction between shallow groundwater, peridotite, and the atmosphere, while high pH, Ca, and OH^--rich fluids evolve from Mg-HCO_3 fluids via carbonate precipitation during continued reaction with peridotite in systems closed to exchange with the atmosphere.

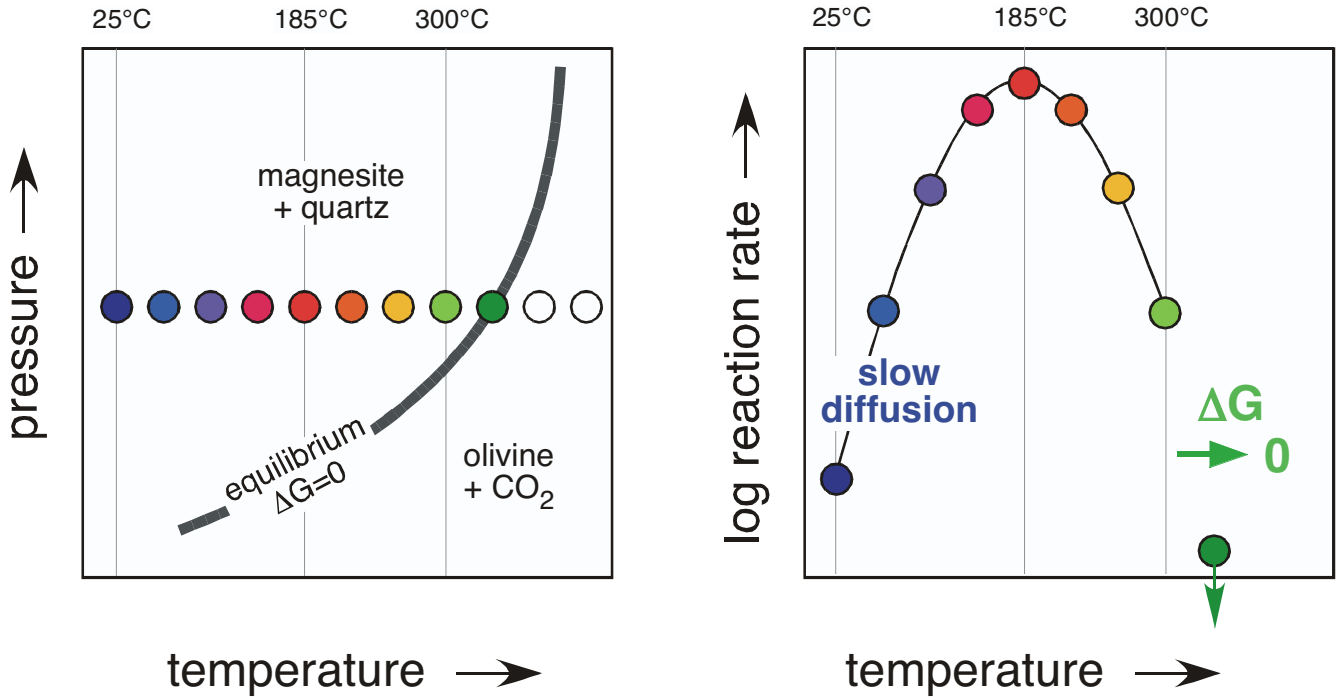

Fig. S3. Schematic illustration of the carbonation rate of olivine (Eq. **2a**). At low temperature, the reaction rate is limited by slow diffusion of chemical components. At higher temperature, the chemical potential driving reaction approaches zero at the equilibrium phase boundary. Thus, the maximum reaction rate is at a temperature intermediate between surface conditions and the equilibrium phase boundary. For experimental data illustrating this point, see Gerdemann *et al.* (Second Annual Conference on Carbon Sequestration, Alexandria, VA, May 5–8, 2003. Report no. DOE/ARC-2003-018, OSTI ID: 898299 8 pp).

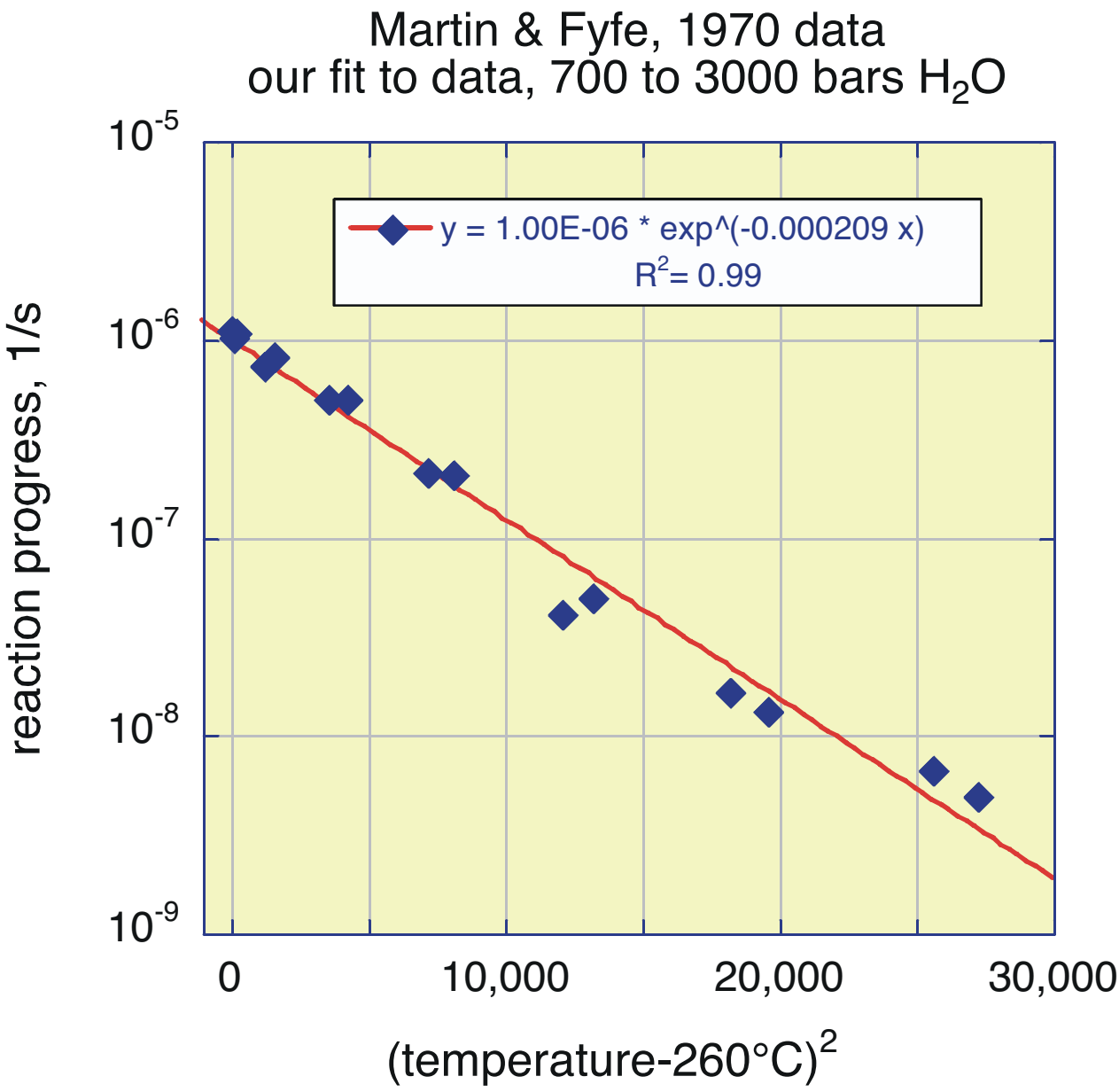

Fig. S4. Our fit to the data of Martin and Fyfe (29) on serpentinization of 58–79 μm olivine powder at 700–3,000 bars of H_2O pressure.

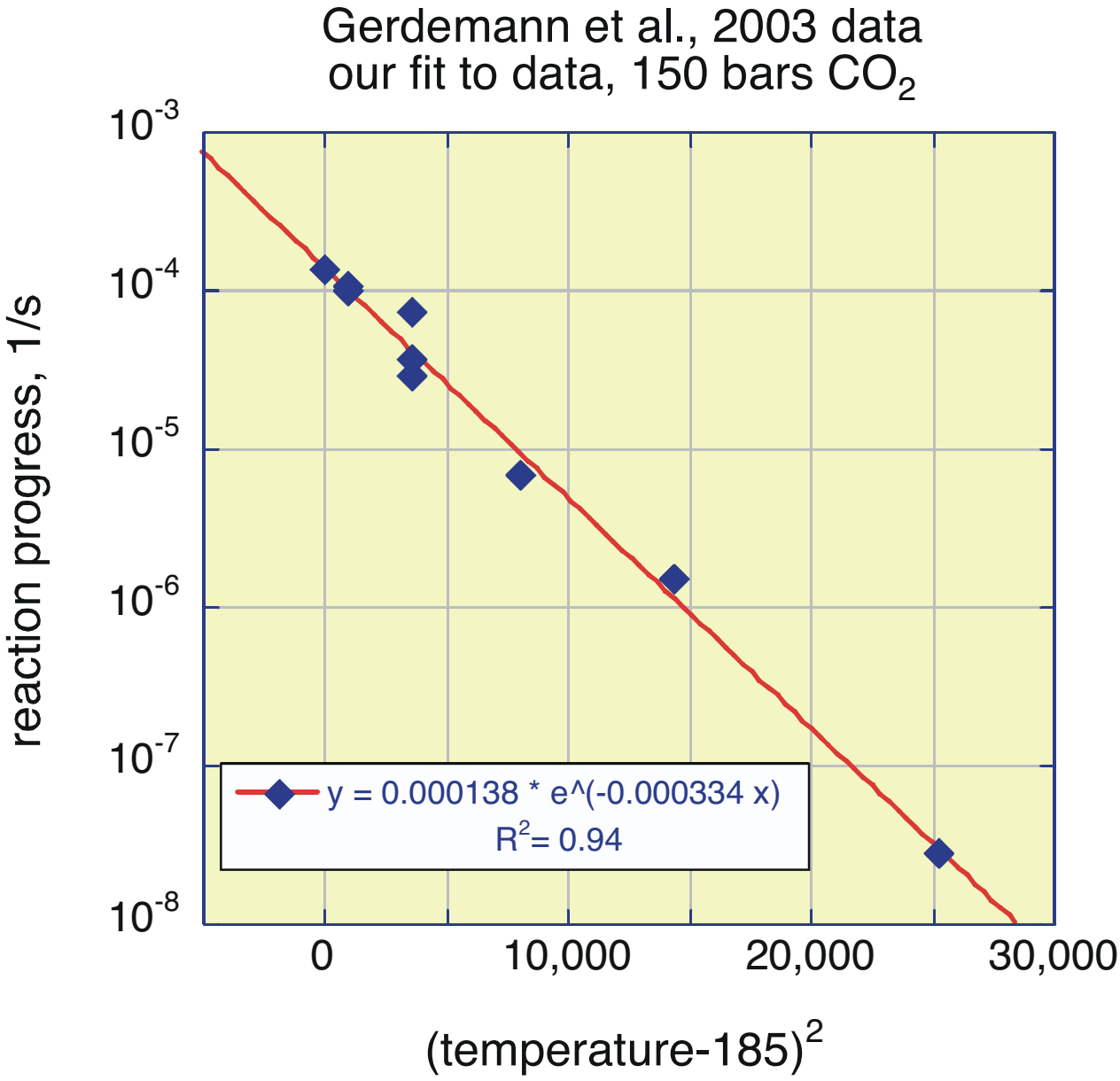

Fig. S5. Our fit to the data of Gerdemann *et al.* (Second Annual Conference on Carbon Sequestration, Alexandria, VA, May 5–8, 2003. Report no. DOE/ARC-2003-018, OSTI ID: 898299 8 pp) on carbonation of <75 μm olivine powder at 150 bars CO_2.

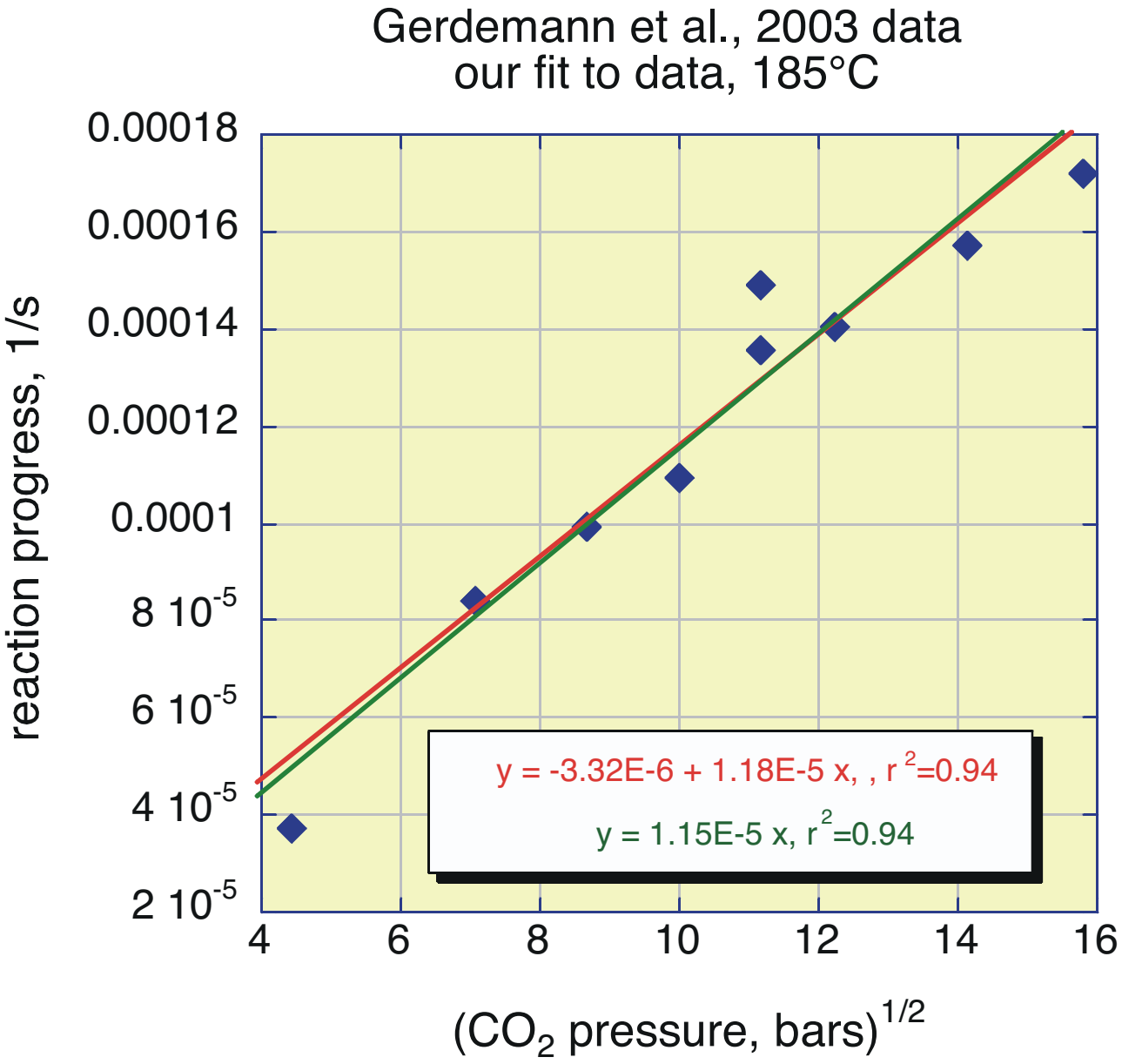

Fig. S6. Our fit to the data of Gerdemann *et al.* (Second Annual Conference on Carbon Sequestration, Alexandria, VA, May 5–8, 2003. Report no. DOE/ARC-2003-018, OSTI ID: 898299 8 pp) on carbonation of <75 μm olivine powder at 185°C.

Table S1. Summary of new 14C geochronology data with sample locations and compositions

Our sample no.	NOSAMS accession no.	Sample type	Location	Description	Latitude, °N	Longitude, °E	Elevation, m	Fraction modern. C	Frac mod uncertainty	^{14}C age, yrs	Age uncertainty, yrs	δ^{13}C ‰, VPDB	Travertine or vein	Minerals most to least abundant, *<10% in italics*
OM07–01	OS-60068	fragments	mtns betw Muttrah & Muscat	carbonate vein on fault in Muscat	23.616	58.574	≈ 115	0.0494	0.0006	24,200	100	−5.56	vein	
OM07–02	OS-60117	fragments	mtns betw Muttrah & Muscat	carbonate vein on fault in Muscat	23.616	58.574	≈ 115	0.0251	0.0008	29,600	250	−10.14	vein	
OM07–03	OS-60071	fragments	Wadi Bani Karous/Al Abyad	carbonate vein on fault	23.39018	57.65915	307	0.0063	0.0004	40,700	460	−7.47	vein	
OM07–04	OS-60074	fragments	Wadi Bani Karous/ Al Abyad	some alteration associated with carbonate veins	23.43000	57.66816	269	0.0113	0.0004	36,000	280	2.5	vein	
OM07–05	OS-59332	powder	Sohar to Wuqbah highway	carbonate veins in serpentine	23.98770	56.52079	417	0.0171	0.0004	32,700	190	−6.17	vein	dol,serp, *cct,grn*
OM07–07	OS-59337	powder	Sohar to Wuqbah highway	carb vein in serpentine, massive compared to 05,≤ 10 cm thick	23.97561	56.50196	472	0.0050	0.0002	42,600	360	−9.72	vein	mag,*dol*
dup OM07–07	OS-60072	fragments	Sohar to Wuqbah highway	carb vein in serpentine	23.97561	56.50196	472	0.0203	0.0004	31,300	160	−9.55	vein	mag,*dol*
OM07–08	OS-60013	powder	village of Jill	erosional remnant above level of travertine terrace	22.86339	57.51501	483	0.0066	0.0003	40,400	310	−15.93	trav	cct,*serp*
dup OM07–08	OS-60191	fragments	village of Jill	erosional remnant above level of travertine terrace	22.86339	57.51501	483	0.0094	0.0003	37,500	260	−15.74	trav	cct,*serp*
OM07–09	OS-60110	powder	village of Jill	2 m below 08 on currently active travertine	22.86339	57.51501	482	0.0369	0.0005	26,500	120	−16.51	trav	
OM07–10	OS-60021	fragments	village of Jill	small globular carbonate on top of the travertine sequence	22.86339	57.51501	482	0.7460	0.0040	2,350	40	−27.21	trav	
OM07–11B	OS-60076	fragments	village of Jill	three different stalactites one meter below 09	22.86300	57.51475	481	0.7535	0.0027	2,270	30	−22.8	trav	
OM07–12	OS-60069	powder	village of Jill	carbonate veins in serpentine, 1 m below stalagtites	22.86300	57.51476	481	0.0277	0.0005	28,800	150	−12.3	vein nr trav	cct,*serp*
OM07–13	OS-60070	powder	village of Jill	between 11 and 12	22.86302	57.51478	482	0.0163	0.0003	33,100	140	−9.91	trav	cct,serp,*grn*
OM07–14	OS-60015	powder	village of Jill	very base of outcrop area, in wadi	22.86274	57.51494	478	0.6328	0.0023	3,670	30	−3.36	trav	cct,serp,dol, *qtz,kao,grn*
OM07–16	OS-59338	powder	''Duck'' outcrop	top of eroded outlier in travertine terrace	22.81464	57.83808	≈ 480	0.0105	0.0003	36,600	240	−12.44	trav	cct,serp,dol, *grn,kao*
OM07–17	OS-60118	powder	''Duck'' outcrop	carbonate vein in serpentine	22.81464	57.83808	≈ 480	0.4901	0.0020	5,730	35	−0.12	vein nr trav	dol,cct,serp, *grn,kao*
OM07–18	OS-60016	powder	''Duck'' outcrop	travertine forming now	22.81464	57.83808	≈ 480	0.8159	0.0027	1,630	25	−17.19	trav	cc,*dol,qtz,grn*
OM07–26	OS-60111	fragments	settlment of Tuf	botryoidal carbonate weathering out of carb veins in serpentine	23.105	57.957	≈ 900	0.0404	0.0006	25,800	130	−7.78	vein	
OM07–27	OS-59339	powder	settlment of Tuf	massive carbonate in wadi assoc w big (≤ 1 m) veins	23.10807	57.95787	917	0.0041	0.0002	44,100	340	−5.46	vein	dol,serp,*cct, grn,kao*

Our sample no.	NOSAMS accession no.	Sample type	Location	Description	Latitude, °N	Longi-tude, °E	Eleva-tion, m	Fraction modern. C	Frac mod uncertainty	^{14}C age, yrs	Age uncertainty, yrs	δ^{13}C ‰, VPDB	Travertine or vein	Minerals most to least abundant, *<10% in italics*
dup OM07–27	OS-60020	fragments	settlment of Tuf	massive carbonate in wadi	23.10807	57.95787	917	0.0101	0.0003	36,900	270	−6.28	vein	dol,serp,*cct, grn,kao*
OM07–28C	OS-60077	fragments	settlment of Tuf	low angle carbonate vein dipping 25–30° SW	23.09935	57.95248	883	0.0515	0.0006	23,800	90	−6.45	vein	
OM07–30A	OS-60019	powder	settlment of Tuf	travertine or dipslope vein in gully below Tuf	23.09935	57.95248	883	0.0118	0.0003	35,600	220	−7.34	trav or vein	dol,cct,serp, *kao,grn*
OM07–30B	OS-60112	powder	settlment of Tuf	dark grey limestone blocks within travertine or vein	23.09935	57.95248	883	0.0845	0.0008	19,850	75	0.36	trav	cct,*grn, serp,kao*
OM07–32	OS-60116	fragments	village of Falaij	carbonate veins in serpentinized perid nr 34	22.84609	58.05617	551	0.3836	0.0018	7,700	35	−7.39	vein	
OM07–34A	OS-59333	powder	village of Falaij	old travertine, 1.5 m above current spring level, big piece	22.84609	58.05617	551	0.1367	0.0011	16,000	65	−11.22	trav	cct,*serp,dol*
dup OM07–34A	OS-60138	fragments	village of Falaij	old travertine, 1.5 m above spring	22.84609	58.05617	551	0.0742	0.0008	20,900	90	−13.64	trav	cct,*serp,dol*
OM07–34B	OS-60139	fragments	village of Falaij	small carbonate vein in perid below travertine deposits	22.84609	58.05617	551	0.4521	0.0019	6,380	35	−6.3	vein	
OM07–34C	OS-60113	powder	village of Falaij	flakes of currently forming travertine	22.84609	58.05617	551	1.1296	0.0043	0		−25.55	trav	cct,*dol,kao,grn*
OM07–39	OS-59336	powder	Wadi Lufti	50 cm carbonate vein in wadi wall	23.24827	58.30994	600	0.0191	0.0003	31,800	140	−8.39	vein	mag,dol,*serp*
OM07–52	OS-59998	fragments	Wadi Nassif	serp & carb veins 5 cm thick in perid	22.908	58.374	≈ 710	0.4146	0.0029	7,070	55	−7.34	vein	
OM07–53	OS-60018	powder	Wadi Nassif	carb vein in dunite, low angle dip	22.908	58.374	≈ 710	0.0056	0.0002	41,700	340	−8.1	vein	
OM07–54	OS-59334	powder	pass betw W Khafifah & W Dima	carbonate coating/veins on joints	22.93592	58.42621	748	0.0086	0.0003	38,200	300	−2.78	vein	dol,serp, *kao,grn*
OM07–56	OS-60114	fragments	pass betw W Khafifah & W Dima	coarse, green serpentine + carbonate vein 1 cm wide	22.93592	58.42621	748	0.0358	0.0008	26,700	170	−4.83	vein	
OM07–57	OS-60067	fragments	pass betw W Khafifah & W Dima	mixed serpentine and carbonate, cm scale veins	22.93592	58.42621	748	0.0052	0.0002	42,200	350	−7.35	vein	
OM07–58	OS-60115	fragments	pass betw W Khafifah & W Dima	perid with mm scale carbonate on joints	22.94071	58.44178	915	0.2606	0.0014	10,800	40	−4.34	vein	

Our sample no.	NOSAMS accession no.	Sample type	Location	Description	Latitude, °N	Longi-tude, °E	Eleva-tion, m	Fraction modern. C	Frac mod uncertainty	^{14}C age, yrs	Age uncertainty, yrs	δ^{13}C ‰, VPDB	Travertine or vein	Minerals most to least abundant, *<10% in italics*
OM07–59	OS-59335	powder	Wadi Dhuli	4 mm carbonate chips in serpentine	22.98407	58.63310	414	0.2221	0.0012	12,100	45	−0.13	vein	
dup OM07–59	OS-60078	fragments	Wadi Dhuli	4 mm carb potato chips in serp	22.98407	58.63310	414	0.1459	0.0013	15,450	70	1.59	vein	
OM07–60	OS-59340	powder	nr ctr of universe	travertine or low angle vein grading into carbonated dunite	22.93906	58.66805	497	0.0185	0.0004	32,000	170	−11.91	vein or trav	dol,mag, serp,*grn*
OM07–61A	OS-59341	powder	Batin camp	erosional remnant of massive, low angle vein	22.92564	58.67109	522	0.0275	0.0004	28,900	110	−7.76	vein	mag,dol
dup OM07–61A	OS-60075	fragments	Batin camp	erosional remnant of massive, low angle vein	22.92564	58.67109	522	0.0099	0.0004	37,000	340	−8.35	vein	mag,dol
OM07–61B	OS-60017	powder	Batin camp	different textural types near top of spine leading SW from 61A	22.92564	58.67109	522	0.1526	0.0012	15,100	65	−0.88	vein	
OM07–61C	OS-60079	powder	Batin camp	different textural types near top of spine leading SW from 61A	22.92564	58.67109	522	0.1123	0.0010	17,550	75	−2.12	vein	dol,mag,*grn,serp*

Samples were analyzed for ^{14}C age determination at the National Ocean Sciences Accelerator Mass Spectrometry Facility in Woods Hole, Massachusetts (NOSAMS). Samples were washed in dilute HCl and broken into ≈ 5 mm sized fragments, after which some were ground to powder in an agate mill, prior to shipment to NOSAMS. At NOSAMS, samples were directly hydrolyzed with strong acid, H_3PO_4, to convert the carbon in the sample to CO_2. Carbon dioxide was reacted with a catalyst to form graphite. An Fe/H_2 catalytic-reduction was used. Graphite was pressed into targets, which were analyzed on the accelerator along with standards and process blanks. Two primary standards were used during all ^{14}C measurements: NBS Oxalic Acid I (NIST-SRM-4990) and Oxalic Acid II (NIST-SRM-4990C). The ^{14}C activity ratio of Oxalic Acid II (δ13C = −17.3 per mil) to Oxalic Acid I (δ13C = −19.0 per mil) was taken to be 1.293. Every group of samples processed included a blank which was analyzed concurrently with the group. The process blank material was IAEA C-1 Carrera marble.

Fraction Modern (Fm) is a measurement of the deviation of the ^{14}C/C ratio of a sample from ''modern.'' Modern is defined as 95% of the radiocarbon concentration (in AD 1950) of NBS Oxalic Acid I normalized to δ^{13}CVPDB = −19 per mil (Olsson, Nobel Symposium, 12th Proc., John Wiley & Sons, New York, p. 17, 1970). AMS results are calculated using the internationally accepted ''modern value'' of $1.176 \pm 0.010 \times 10^{-12}$ (Karlen et. al. Absolute determination of the activity of two ^{14}C dating standards. Arkiv Geofysik 4, 465–471, 1968) and a final ^{13}C correction is made to normalize the sample Fm to a δ^{13}CVPDB value of −25 per mil. Stable isotope measurements of sample δ^{13}C used to correct Fm values were made at the NOSAMS Facility by analyzing sub-samples of the CO_2 gas generated during graphite production with either a VG PRISM or VG OPTIMA mass spectrometer.

Reporting of ages and/or activities follows the convention outlined by Stuiver and Polach (Discussion: Reporting of ^{14}C data. Radiocarbon, 19, 355–363, 1977) and Stuiver (Workshop on ^{14}C data reporting. Radiocarbon, 22, 964, 1980). Radiocarbon ages are calculated using 5568 yrs as the half-life of radiocarbon and are reported without reservoir corrections or calibration to calendar years.

Atoms of ^{14}C contained in a sample are directly counted using the AMS method of radiocarbon analysis, therefore, internal statistical uncertainty is calculated using the number of counts measured from each target. An external precision is calculated from the reproducibility of individual analyses for a given target. The uncertainty reported is the larger of the internal or external uncertainty.

Proportion of minerals was determined using a combination of X-Ray Flourescence analyses for major element composition (Washington State University) and X-Ray Diffraction (at Woods Hole OceanographicInstitution, by Margaret Sulanowska) on powders, with data analaysis using Mac-Diff software. Proportions were determined by Lisa Streit using least squares mass balance of the XRF data, beginning with the mineral identifications from XRD. Minerals listed are dolomite (dol), calcite (cct), magnesite (mag), chrysotile (serpentine polymorph, serp), quartz (qtz), greenalite (grn), and kaolinite (kao). Some of these mineral identifications are uncertain, so that other Mg-Ca carbonates such as huntite may be present instead of or in addition to dolomite + calcite, and serpentine polymorphs, clays and other hydrous silicates may be present instead of or in addition to greenalite and kaolinite. In preliminary electron microprobe analyses we have identified carbonates with Ca/Mg intermediate between calcite and dolomite, as reported for some veins and travertines in California (Barnes & O'Neil, Geochim. Cosmochim. Acta, 51, 699–713, 1951) and Oman (Stanger & Neal, Chem. Geol. 112, 247–254, 1994). Away from currently forming travertines, veins are dominantly dolomite and magnesite; within a few meters of currently forming travertines, veins contain abundant calcite ± dolomite; travertines are dominated by calcite.

Table S2. Transects of carbonate vein thickness in peridotite outcrops

					UTM Zone 40Q		
	Transect length, mm	Total vein thickness, mm	% veins	no. veins	UTM E	UTM N	Elevation, m
Far from active springs							
roadcutjohn1	29,171	229	0.79%	25	647827	2537677	912
roadcutjohn2	8,080	82	1.01%	12	647827	2537677	912
roadcutpeter1	10,040	22	0.22%	43	647967	2537823	884
roadcutpeter2	10,750	148.3	1.38%	47	647942	2537818	902
Totals	58,041	481.3		127			
Length-weighted average proportion		0.83%					
Near springs							
duckgreg1	4,120	193	4.68%	25	586213	2523342	≈520
duckgreg2a	1,110	122	10.99%	19	586112	2523167	≈520
duckgreg2b	370	42	11.35%	7	586112	2523167	≈520
duckgreg3	3,950	216	5.47%	54	586400	2523275	≈520
duckpeter1	7,775	270.75	3.48%	102	586383	2523255	≈520
duckpeter2	745	88	11.81%	24	586154	2523325	≈520
spring1	3,219	190	5.90%	76	530058	2542632	≈575
spring2	2,524	104	4.12%	49	530058	2542632	≈575
Totals	23,813	1225.75		251			
Length-weighted average proportion		5.15%					